Multikernel Graph Structure Learning for Multispectral Point Cloud Classification

Qingwang Wang, *Member, IEEE*, Zifeng Zhang, Jiangbo Huang, *Graduate Student Member, IEEE*, Tao Shen, *Member, IEEE*, and Yanfeng Gu, *Senior Member, IEEE*

***Abstract*—Multispectral point cloud, with spatial and multiple-band spectral information, provides the data basis for finer land cover 3-D classification. However, spectral information is not well utilized by traditional methods of point cloud classification. Benefiting from the excellent performance of graph neural networks on non-Euclidean data, it is well suited to the joint use of spatial and spectral information from multispectral point clouds to achieve better classification performance. However, existing graph-based methods for point cloud classification rely on manual experience to construct input graph and cannot adapt to the complexity of remote sensing scenes. In this article, we propose a novel multikernel graph structure learning (MKGSL) framework for multispectral point cloud classification. Specifically, we explore the high-dimensional feature distribution properties of multispectral point clouds in Hilbert space through the use of kernel method. An innovative multiple-kernel learning mechanism is embedded into our network, which allows to obtain better mappings adaptively. Simultaneously, a series of prior constraints designed based on land cover distribution characteristics are imposed on the network training process, which leads the learned graph of the multispectral point cloud to facilitate better classification. Our method is dedicated to adaptively constructing task-oriented graph structures to improve the performance of multispectral point cloud classification. Experimental comparisons demonstrate that the proposed MKGSL performs better than several state-of-the-art methods on two real multispectral point cloud datasets.**

***Index Terms*—Graph structure learning, multiple kernel learning, multispectral LiDAR data, point cloud classification, prior constraint.**

I. Introduction

LAND cover classification has long been a fundamental and challenging topic in the field of remote sensing. The advent of airborne multispectral LiDAR systems has provided new opportunities for this field by enabling the acquisition of both spatial coordinates and spectral information of sampled points on the terrain surface in the survey area. This simultaneous collection of spatial and spectral data results in the formation of multispectral point clouds, which serve as a direct representation of the three-dimensional (3-D) land covers. The availability of multispectral point cloud data provides the necessary foundation and information for achieving finer 3-D classification of land cover [1]. By leveraging the rich spatial and spectral information embedded in these data, a more comprehensive understanding of the land cover distribution can be obtained, enabling more accurate and detailed classification of land cover.

However, multispectral point clouds exhibit an irregular distribution property, rendering them unsuitable for direct processing using traditional matrix-based methods that are typically employed for regular Euclidean data. Consequently, specialized modeling and characterization techniques are required to effectively integrate the 3-D spatial–spectral information present in multispectral point clouds. In order to enhance land cover classification performance using multispectral point clouds, it is imperative to develop advanced techniques that can effectively model and analyze these data. This involves addressing the challenges posed by their irregular distribution and developing novel methodologies that can exploit the joint spatial and spectral information for improved classification accuracy and detail.

Existing research works on multispectral point cloud classification can be summarized into two technological routes: pixel-oriented image processing and point-oriented point cloud processing techniques [2]. Pixel-oriented image processing methods convert point clouds into 2-D images for processing, which inevitably leads to a loss of 3-D spatial information. Traditional point-oriented methods cannot make good use of spectral information of multispectral point clouds. Therefore, it is necessary to propose new methods for the integration of 3-D spatial and spectral information of multispectral point cloud.

With the development of graph theory in the field of deep learning, the utilization of graph methods to point cloud related applications is gradually emerging. Graphs have the natural advantage of being a representation of the complex relationships and interdependencies between objects [3]. According to the Tobler's first law of geography, the relationship between features of land covers is an important basis for classification, making the graph method naturally suitable for classifying point clouds. However, most of the existing research works only use

Manuscript received 19 January 2024; revised 7 February 2024; accepted 15 February 2024. Date of publication 22 February 2024; date of current version 6 March 2024. This work was supported in part by the National Natural Science Foundation of China under Grant 62201237 and Grant 42067029, in part by the Yunnan Fundamental Research Projects under Grant 202101BE070001-008 and Grant 202301AV070003, in part by the Youth Project of the Xingdian Talent Support Plan of Yunnan Province under Grant KKRD202203068, and in part by the Major Science and Technology Projects in Yunnan Province under Grant 202202AD080013 and Grant 202302AG050009. *(Corresponding author: Tao Shen.)*

Qingwang Wang, Zifeng Zhang, Jiangbo Huang, and Tao Shen are with the Faculty of Information Engineering and Automation, Kunming 650500, China, and also with the Yunnan Key Laboratory of Computer Technologies Application, Kunming University of Science and Technology, Kunming 650500, China (e-mail: wangqingwang@kust.edu.cn; 20212104057@stu.kust.edu.cn; jiangbohuang@stu.kust.edu.cn; shentao@kust.edu.cn).

Yanfeng Gu is with the School of Electronics and Information Engineering, Harbin Institute of Technology, Harbin 150001, China, and also with the Heilongjiang Province Key Laboratory of Space-Air-Ground Integrated Intelligent Remote Sensing, Harbin 150001, China (e-mail: guyf@hit.edu.cn).

Digital Object Identifier 10.1109/JSTARS.2024.3368472

the 3-D spatial nearest-neighbor relationship of multispectral point clouds to construct graph models, without making full use of the spatial–spectral information for scene adaptive graph construction.

To address the above-mentioned issues, we propose a kernel-based method to construct a scene adaptive graph structure by using multiple Gaussian kernels that jointly exploit the spatial–spectral information of multispectral point clouds. A series of prior constraints are imposed to guide the optimization of the multikernel graph structure based on Tobler's first law of geography simultaneously. This leads to a better classification performance for multispectral point cloud. More specifically, the main contributions can be summarized as follows.

1) A multikernel graph structure learning (MKGSL) framework is proposed for the classification of multispectral point clouds. First, adaptive multiscale relationships within the multispectral point cloud are acquired through the learning of graph combinations. Then, the graphs are further refined by incorporating a series of *a priori* constraints to better conform to the inherent properties of the multispectral point cloud. Throughout the network training process, the graph undergoes dynamic modifications.
2) A multikernel learning mechanism is incorporated into the framework of graph neural networks (GNNs), with the aim of enhancing the capacity of the model in representing nonlinear information. By autonomously learning the weights for the linear combination of multiple kernels, the model becomes adaptive to different scenes, thereby increasing its effectiveness in capturing complex relationships.
3) The low-rank, sparse, and feature smooth prior constraints are designed based on manual experience to guide the optimization of the graph structure, aiming to better fit the classification task and reflect the higher order essential properties of multispectral point clouds.

The rest of this article is organized as follows. Section II briefly describes existing point cloud classification methods and the applications of graph theory in point cloud classification. Section III details the methodological principles and implementation process of MKGSL. Section IV verifies the advantages of MKGSL by comparing the performance of different graph construction methods. Finally, Section V concludes this article with some remarks and presents the perspective of future work.

II. Related Works

As multispectral LiDAR moves from laboratory research to practical application, it realizes the 3-D spatial–spectral integrated information acquisition of observation scenes. It provides data support for the spatial 3-D classification of remote sensing land covers. In this section, we describe the works in terms of existing methods to the exploitation of multispectral point clouds, as well as graph-based classification methods.

A. Existing Methods of Point Cloud Classification

Existing works on point cloud classification can be broadly divided into two categories, i.e., pixel-oriented classification methods, and point-oriented classification methods.

Pixel-oriented image processing technique typically converts a point cloud to feature images. Discriminatory information on land covers is then extracted from the feature images using traditional methods, such as Mahalanobis distance classifiers [4], maximum likelihood classifiers [5], support vector machines [2], [6], [7], [8], decision tree [9], random forest analysis [10], deep Boltzmann machine [11], and deep learning [12], [13]. And it has been shown that deep learning-based methods can achieve better classification performance [12]. Some scholars have targeted convolutional neural network (CNN) model optimization for multispectral LiDAR feature images and further proposed a hybrid capsule network based on the coding–decoding structure as well as a self-attention capsule module [14].

Point-oriented processing technique treats the multispectral point cloud as an extension of the traditional point cloud. The methods directly perform pointwise classification without data conversion [15]. Analyzing the spectral information of multispectral point cloud, it was found that multispectral point clouds are suitable for 3-D fine classification of land covers in remote sensing scenes. From using spatial and spectral information separately to joint use for point cloud classification [16], [17], some scholars have further proposed multispectral point cloud classification methods based on multiscale spatial and spectral feature selection [17]. For example, transformer was introduced in the multispectral point cloud classification task [18], [19]. Wang et al. [15] proposed a 3-D land cover classification method based on the tensor representation. Currently, some scholars are beginning to focus on designing deep neural networks for multispectral point clouds, and implementing optimization based on PointNet [20], [21], [22].

B. Applications of Graph Theory for Multispectral Point Cloud Classification

CNNs have achieved notable success in areas, such as image recognition, but CNN can only handle regular Euclidean data and cannot directly handle non-Euclidean data, such as graphs. Moreover, graph is a generalized data structure that grid and sequence can be viewed as a special case of. As typical non-Euclidean data, multispectral point clouds are difficult to be processed directly by networks based on Euclidean data, such as CNN. As a result, scholars have modeled multispectral point clouds with graph theory [3], [23], [24], [25], [26], [27], [28], and started to design GNNs for feature extraction and classification of multispectral point clouds.

Similar to CNNs, graph convolutional network (GCN) [29], [30], a typical GNN, also has a powerful learning capability through graph convolutional operation. And some scholars have used the attention mechanism to propose graph attention networks (GATs) to solve the problem that GCN cannot assign weights to nodes [31]. For the oversmoothing problem of GCN, some scholars introduced initial residual and identity mapping

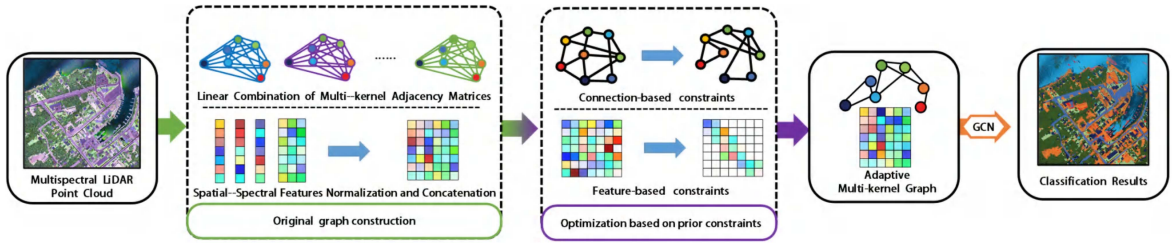

Fig. 1. Adaptive graph structure learning framework.

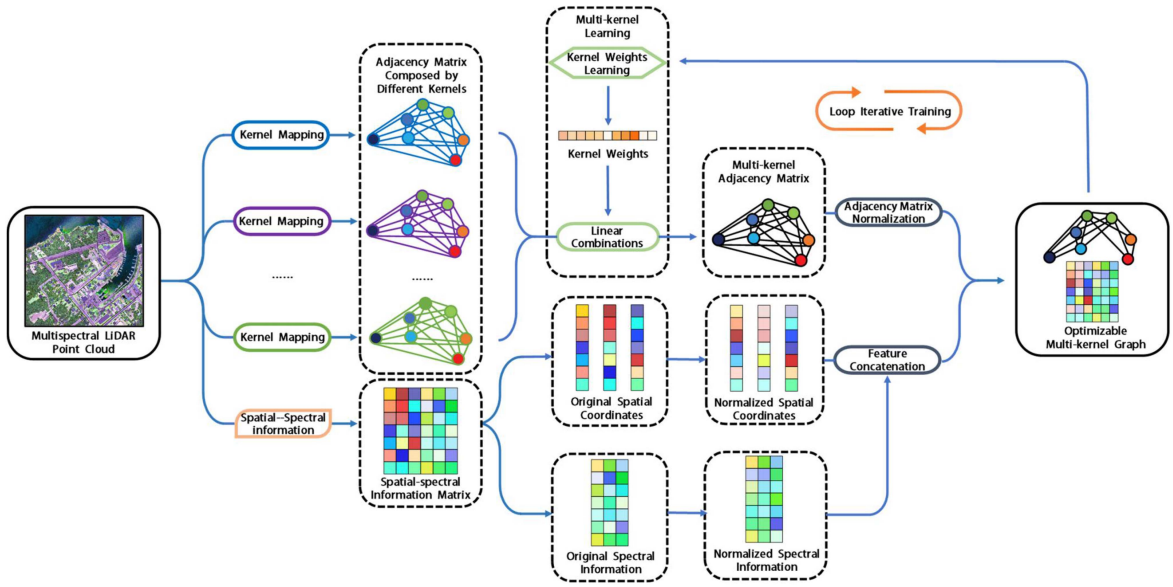

Fig. 2. Process of MKGSL.

to propose GCNII [32]. Recently GCN has been successfully applied to the field of remote sensing. Li et al. [33] proposed a GCN-based method for extracting power lines and pylons. Chen et al. designed auto-GCN to dynamically learn graph structure characterization of hyperspectral images to achieve better classification. Inspired by this, as multispectral point clouds are typically non-Euclidean data, similar work could be carried out. Wang et al. [24] modeled the multispectral points as a graph and proposed a multiattribute smooth graph convolutional network (MaSGCN) for multispectral point cloud classification. Landrieu et al. argued that superpoint graphs can effectively capture the organization of 3-D point clouds and proposed a deep learning-based method for large-scale point cloud classification. Zhang et al. [34] proposed to introduce a multikernel integrated attention mechanism in GNNs to measure feature similarity in Hilbert space. The above-mentioned graph-based methods inspire us to design a method for point cloud classification using kernel methods for the adaptive construction of multispectral point cloud graph, the details of which are described in the following.

III. Methodology

In this section, we describe the proposed MKGSL framework for multispectral point cloud classification in detail. The multikernel learning is embedded in a graph-based network, which is used to fit a mapping of multispectral point clouds to a high-dimensional feature space by learning a combination of different base kernels. Meanwhile, the evolution of the graph structure is guided by a series of *a priori* constraints derived from the Tobler's first law of geography. The entire process from constructing the graph to implementing the point cloud classification is shown in Fig. 1.

A. Multikernel Graph Construction

Given a multispectral point cloud $\mathbf{X} = \{\mathbf{x}_1, \mathbf{x}_2, \cdots, \mathbf{x}_N\}$ where $\mathbf{x} \in \mathbb{R}^{(3+L)}$ represents a single point with 3-D spatial coordinates and L bands of spectral intensity, and N represents the number of points contained in the point cloud. We use kernel function to measure the similarity of any two points in a multispectral point cloud. Further, a multiple kernel metric of intersample similarity is employed to overcome the limitations of a single kernel for the insufficient nonlinear measurement. To make the multikernel combinatorial function easy to train, we introduce a set of trainable kernel weights $\mathbf{W}_{\text{kernel}} = \{\eta_1, \eta_2, \ldots \eta_M\}$. The general form is as follows:

$$k(\mathbf{x}_i, \mathbf{x}_j) = \sum_{m=1}^{M} \eta_m k_m(\mathbf{x}_i, \mathbf{x}_j) \text{ s.t. } \sum_{m=1}^{M} \eta_m = 1 \quad (1)$$

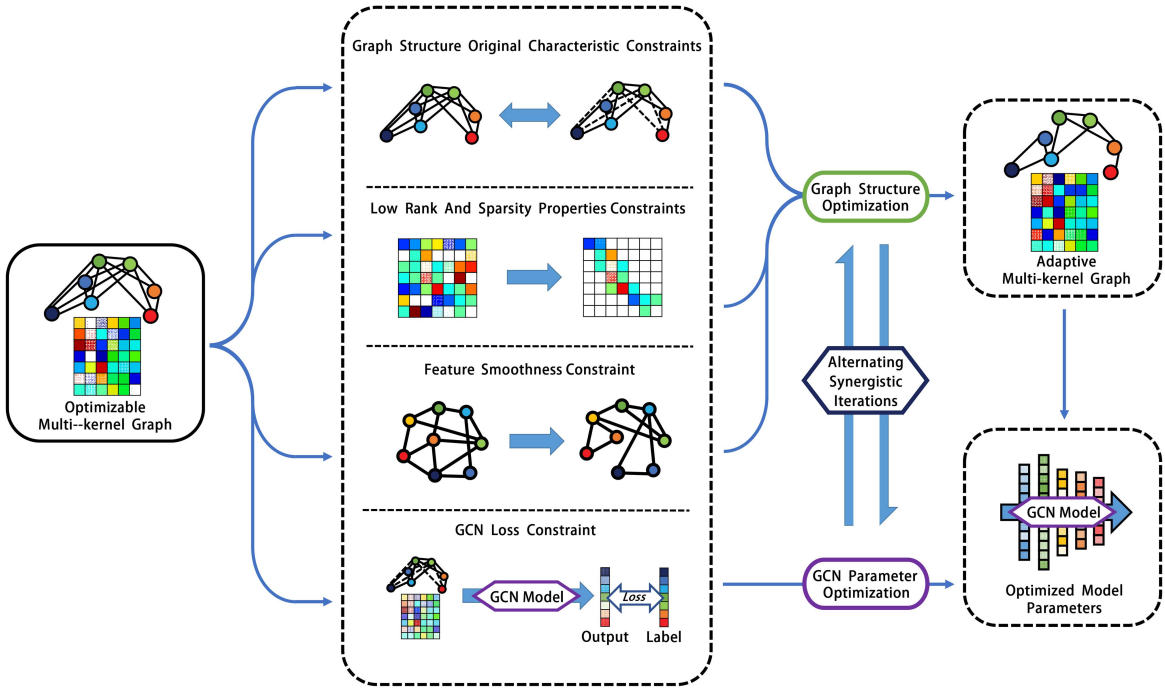

Fig. 3. Optimization of multikernel graph structures with prior constraints.

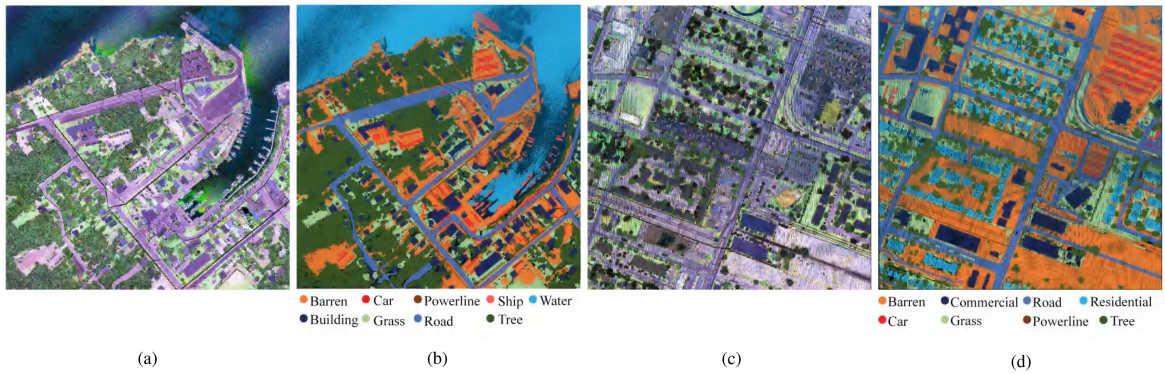

Fig. 4. Visualization and ground truth of multispectral point cloud of two scenes. (a) Harbor of Tobermory (HT). (b) Ground truth of HT. (c) University of Houston (UH). (d) Ground truth of UH.

where k_m is the base kernel, and η_m is the weight of the base kernel. The base kernel is a Gaussian kernel, which is defined as follows:

$$k_m\left(\mathbf{x}_i, \mathbf{x}_j\right) = \exp\left(-\frac{\left\|\mathbf{x}_i - \mathbf{x}_j\right\|_2^2}{2{\sigma_m}^2}\right) \tag{2}$$

where σ_m is the kernel width, which is a hyperparameter that controls the smoothness of the kernel function, and $\|\|_2$ is the Euclidean distance.

Mathematically, the variety of high-dimensional mappings fitted by the kernel function can be substantially extended by a linear combination of different base kernels, which allows to search adaptively in Hilbert space for the most suitable mapping for the task.

We use the softmax function to normalize each row of the constructed adjacency matrix so that the sum of the weights of each point connected to the target point is 1

$$a_{i,j}^m = \exp\left(k_m\left(\mathbf{x}_i, \mathbf{x}_j\right)\right) \Big/ \sum_{j=1}^{N} \exp\left(k_m\left(\mathbf{x}_i, \mathbf{x}_j\right)\right). \tag{3}$$

Since the spatial and spectral features of the multispectral point cloud contain different information and there are large quantitative differences in the value, we measure the similarity separately and form two different adjacency matrices, and combine them in the implementation

$$\mathbf{A}_m = \text{normalized}\left(\mathbf{A}_{\text{Spectral}} + \mathbf{A}_{\text{Spatial}}\right) = \left\{a_{i,j}^m\right\}. \tag{4}$$

The normalized adjacency matrix $\mathbf{A}_m = \{a_{i,j}^m\}$ represents the mth original graph structure of the graph structure learning

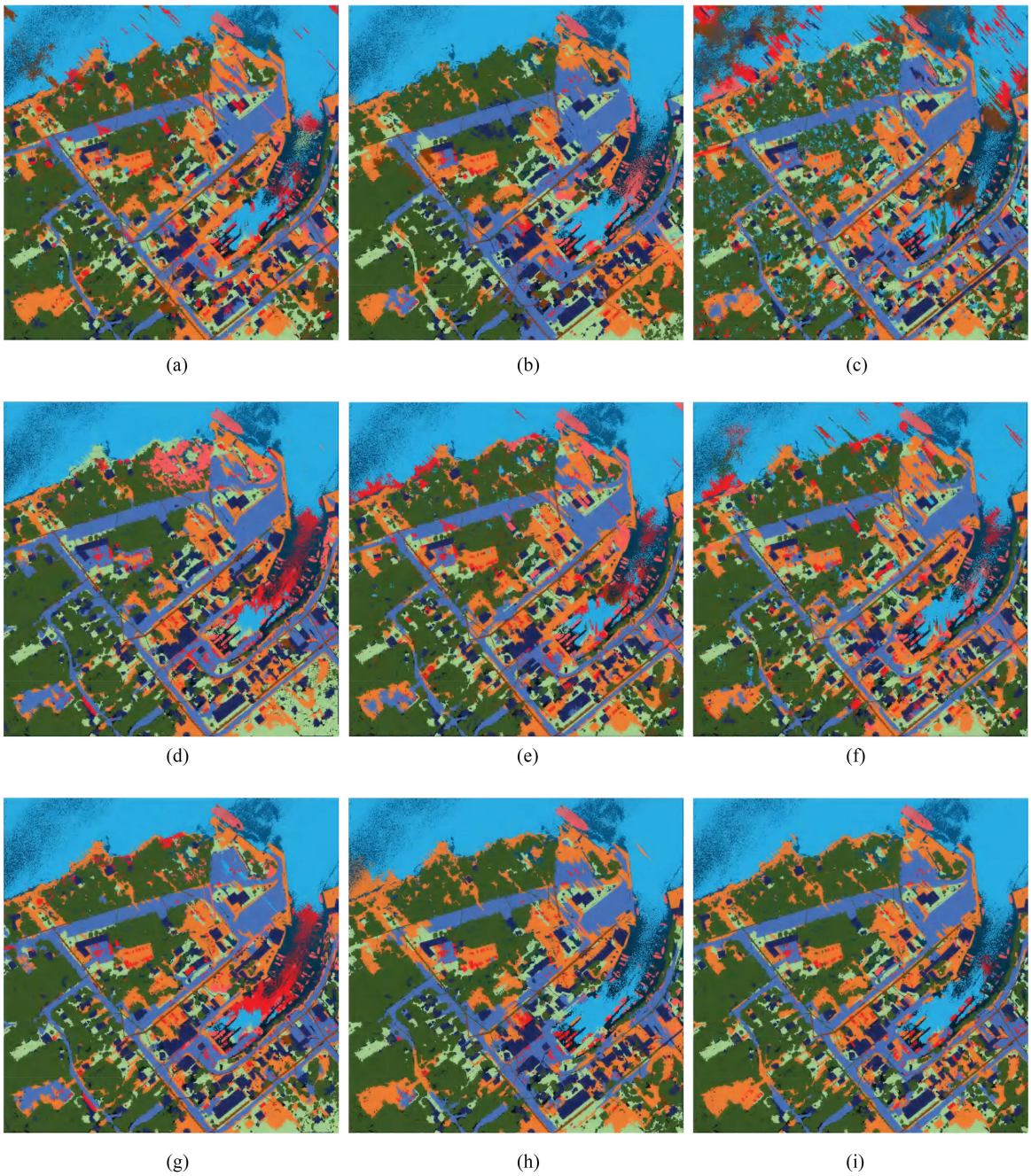

Fig. 5. Visualization of the classification results on HT dataset. (a) GCN-spatial+spectral. (b) GCN-spatial. (c) GCN-spectral. (d) MLP. (e) GCNII. (f) GAT. (g) GCBnet. (h) MaSGCN. (i) MKGSL.

network and $\mathbf{A} = \sum_{m=1}^{M} \eta_m \mathbf{A}_m$ represents the original multispectral point cloud graph. The ith row of the original adjacency matrix of the multispectral point cloud represents the similarity of the ith point to all other points.

After obtaining the original graph structure, we feed it into a GCN for loop iterative training, the overall process is shown in Fig. 2. As the GCN iterates, the weights of base kernels $\mathbf{W}_{\text{kernel}} = \{\eta_1, \eta_2, \ldots \eta_M\}$ are optimized simultaneously. Eventually, the most reasonable set of base kernels combination weights will be learned, so that we obtain the optimal multispectral point cloud multikernel graph.

B. Optimization of Graph Structure With Priori Constraints

The above-mentioned multikernel graph construction focuses on the optimization of global similarity metrics. Given the complexity of the remote sensing scenes and the variability of the nodes, we tend to introduce manual experience. So, we design a series of priori constraints to guide the evolution of the multikernel graph learning. Expect to further optimize the multispectral point cloud graph for the classification task from the perspective of matrix properties and physical implications. The process for optimizing the structure of the multikernel graph with some prior constraints is shown in Fig. 3.

Fig. 6. Visualization of the confusion matrix for classification results on HT dataset. (a) GCN-spatial+spectral. (b) GCN-spatial. (c) GCN-spectral. (d) MLP. (e) GCNII. (f) GAT. (g) GCBnet. (h) MaSGCN. (i) MKGSL.

To enable iterative optimization of the graph structure in the model, we design a free graph structure $\mathbf{S}$ and replicate the multikernel graph structure obtained from the previous learning onto $\mathbf{S}$. For the optimized graph to retain as much information as possible from the original graph, we impose graph structure original characteristic constraint. The difference between the original multikernel graph structure and the replicated new learnable graph structure is measured by calculating the F-norm. Minimizing the F-norm as an optimization constraint can control the graph from deviating too much from the original graph structure during the iteration. In addition, we set a hyperparameter γ to control the contribution of the constraint, preventing the problem of overconstraining, which would make it impossible to optimize.

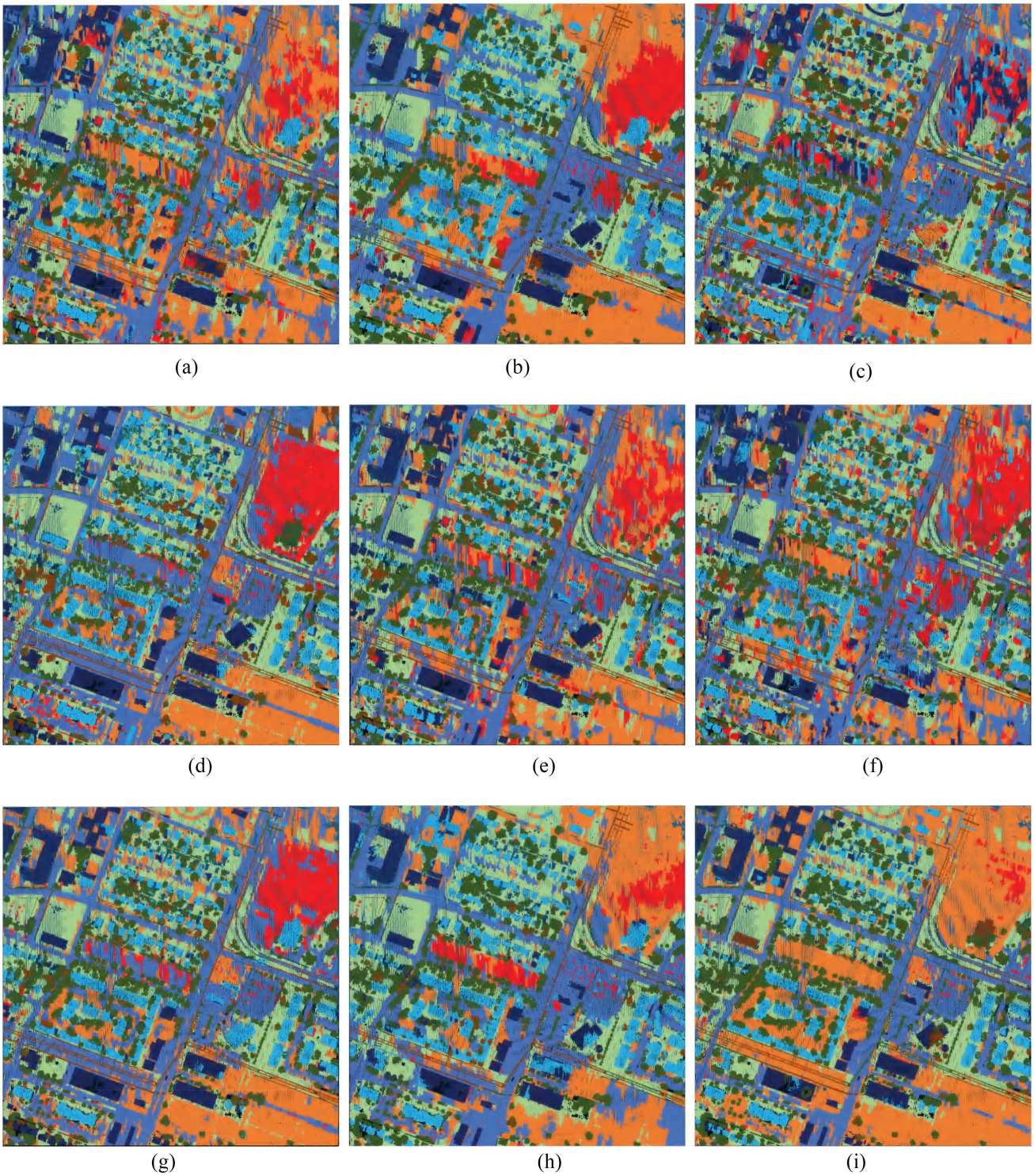

Fig. 7. Visualization of the classification results on UH dataset. (a) GCN-spatial+spectral. (b) GCN-spatial. (c) GCN-spectral. (d) MLP. (e) GCNII. (f) GAT. (g) GCBnet. (h) MaSGCN. (i) MKGSL.

According to the Tobler's first law of geography, the key features for classification can be extracted from the spatial distribution of geographical objects and their attributes. Meanwhile, it is a subset of the point cloud that contributes to the classification of the target points. So the graph structure should be of low rank and sparse.

In order to make the graph structure low-rank and sparse, we impose the $\ell 1$ norm and the nuclear norm constraints on the adjacency matrix during the optimization process. In order to make the graph structure low-rank and sparse, we impose the norm and the nuclear norm constraints on the adjacency matrix during the optimization process.

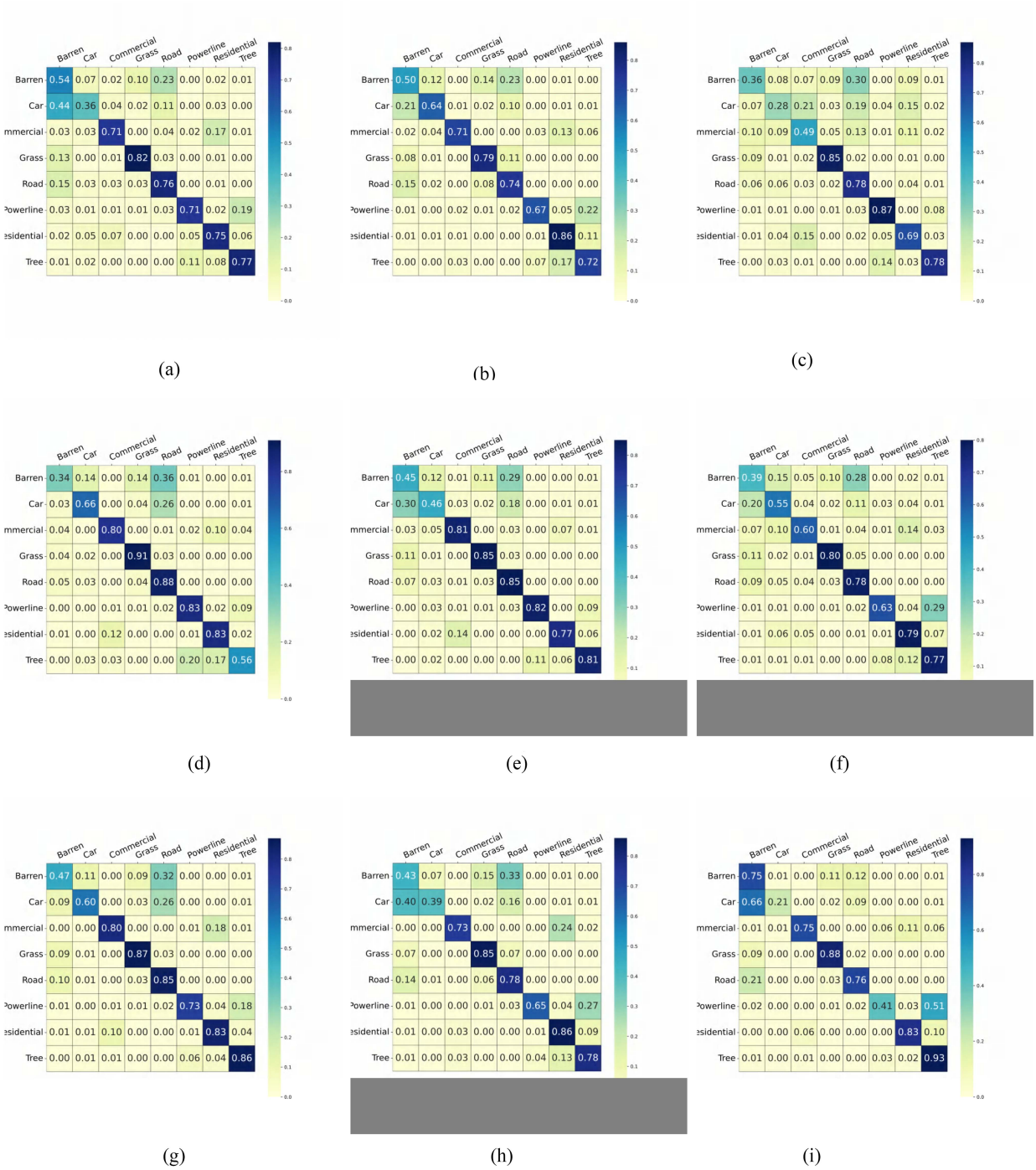

Fig. 8. Visualization of the confusion matrix for classification results on UH dataset. (a) GCN-spatial+spectral. (b) GCN-spatial. (c) GCN-spectral. (d) MLP. (e) GCNII. (f) GAT. (g) GCBnet. (h) MaSGCN. (i) MKGSL.

The learned adaptive graph is used to describe the similarity of the multispectral point cloud, so the features of nodes in the graph should be smooth

$$\mathcal{L}_S = \frac{1}{2}\sum_{i,j}^{N} \mathbf{S}_{ij} \left\|\mathbf{x}_i - \mathbf{x}_j\right\|_F^2 = \mathrm{tr}\left(\mathbf{X}^{\mathbf{T}}\mathbf{L}\mathbf{X}\right) \tag{5}$$

where $\mathbf{S}_{ij}$ denotes the connection weights of fixed point i and j in the graph, $\mathbf{L} = \mathbf{D} - \mathbf{S}$ is the graph Laplace matrix, and $\mathbf{D}$ is the degree matrix of $\mathbf{S}$. We use the normalized Laplacian matrix $\hat{\mathbf{L}} = \mathbf{D}^{-\frac{1}{2}}\mathbf{L}\mathbf{D}^{-\frac{1}{2}}$ to replace $\mathbf{L}$ and obtain the feature smoothing constraint term.

As mentioned at the beginning of this section, a uniform similarity metric is difficult to adapt well to the characteristics of all the different nodes in a complex remote sensing scene. The graphs learned with these prior constraints can aptly overcome this problem, resulting in a better representation of the graph structure for multispectral point cloud classification. The

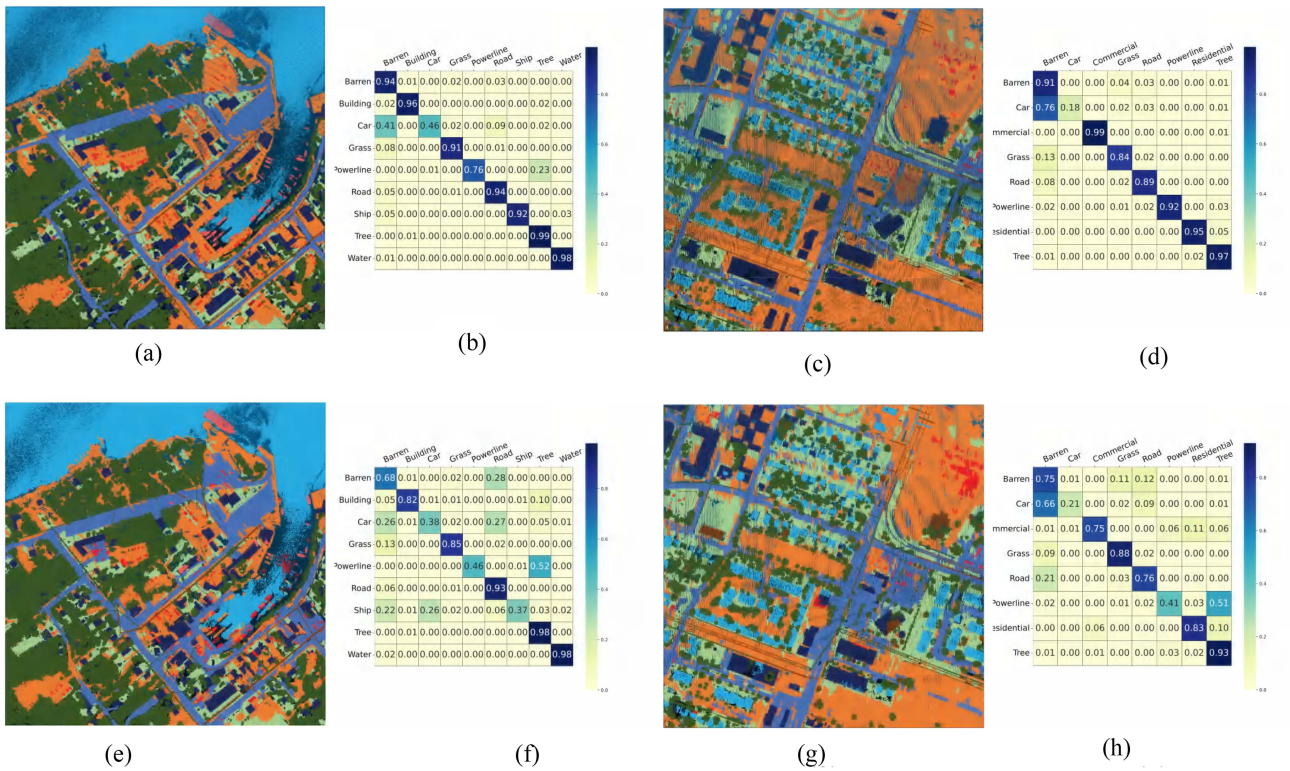

Fig. 9. Visualization of superpoint segmentation compared to classification results. (a) Performance limit on HT. (b) Confusion matrix limit on HT. (c) Performance limit on UH. (d) Confusion matrix limit on UH. (e) MKGSL on HT. (f) Confusion matrix of MKGSL on HT. (g) MKGSL on UH. (h) Confusion matrix of MKGSL on UH.

optimization problem with prior constraints can be expressed as follows:

$$\arg\min_{\mathbf{S}\in\mathbb{Q}} \mathcal{L} = \alpha\|\mathbf{S}\|_1 + \beta\|\mathbf{S}\|_* + \gamma\left\|\sum_{m=1}^{M}\eta_m\mathbf{A}_m - \mathbf{S}\right\|_F^2 + \lambda\mathcal{L}_S + \mathcal{L}_{\text{oss}} \tag{6}$$

where $\|\|_F^2$ is the F-norm, $\|\|_1$ is the $\ell 1$ norm and $\|\|_*$ is the nuclear norm. α, β, γ, and λ are hyperparameters that control the contribution of the constraints. $\mathcal{L}_{\text{oss}}$ is the loss function of the classification, which is a cross-entropy loss function.

C. Adaptive Multikernel Graph-Based Multispectral Point Cloud Classification

We select the GCN network as the base network for multispectral LiDAR point cloud classification. Through the strategy of learning the graph structure and co-optimizing the network model, higher classification accuracy and better adaptive capability of graph model construction can be achieved. In the data preprocessing stage, we map the multispectral point cloud into several adjacency matrices according to different Gaussian kernels with different parameters. In addition to the model weight matrix, a learnable kernel weights vector $\mathbf{W}_{\text{kernel}} = \{\eta_1, \eta_2, \ldots \eta_M\}$ is set up to learn the combinatorial patterns of the multikernel graph structure. To keep the weights of each adjacency matrix nonnegative and the sum of the weights one in each iteration, we flatten the kernel weight vectors to nonnegative values and normalize them before each combination of the multikernel adjacency matrices, and finally assign the processed values back to the trainable parameters.

It is known that the single-layer GCN can be represented as the following form:

$$f_\Theta(\mathbf{X}, \mathbf{A}) = \text{softmax}\,\sigma\left(\mathbf{AXW}\right) \tag{7}$$

where $\mathbf{W} \in \Theta$ is the trainable weight of the model. With the addition of multikernel learning, the output of the model can be expressed in the following form:

$$f_\Theta(\mathbf{X}, \mathcal{A}, \mathbf{W}_{\text{kernel}}) = \text{softmax}\,\sigma\left(\sum_{m=1}^{M}\eta_m\mathbf{A}_m\mathbf{XW}\right) \tag{8}$$

where $\mathcal{A} = \{\mathbf{A}_1, \mathbf{A}_2, \ldots, \mathbf{A}_M\}$ represents the set of adjacency matrices composed of different Gaussian kernels. In the final setup of the network, we use three layers of graph convolution and two layers of MLP [35], which makes the output of our final model the following form:

$$f_{\text{GCN}} = \sigma\left(\sum_{m=1}^{M}\eta_m\mathbf{A}_m\sigma \times\left(\sum_{m=1}^{M}\eta_m\mathbf{A}_m\sigma\left(\sum_{m=1}^{M}\eta_m\mathbf{A}_m\mathbf{XW}_1\right)\mathbf{W}_2\right)\mathbf{W}_3\right) \tag{9}$$

$$f_\Theta(\mathbf{X}, \mathcal{A}, \mathbf{W}_{\text{kernel}}) = \text{softmax}\sigma\left(\mathbf{W}_5\sigma\left(\mathbf{W}_4 f_{\text{GCN}} + \mathbf{b}_1\right) + \mathbf{b}_2\right) \tag{10}$$

where $\Theta = \{\mathbf{W}_1, \mathbf{W}_2, \mathbf{W}_3, \mathbf{W}_4, \mathbf{W}_5, \mathbf{b}_1, \mathbf{b}_2\}$ is the set of trainable parameters in the model. As the model iterates to convergence, we obtain a combination of multikernel adjacency matrices and learn the optimal multikernel graph structure. Further optimization is then achieved by adding the prior constraints to the learned optimal multikernel graph structure. We have thus obtained the optimal multikernel adaptive graph structure. The model eventually outputs the classification results of multispectral point cloud based on the learned adaptive graph.

IV. Experiments

In this section, we conduct experiments to evaluate the performance of the proposed MKGSL for multispectral point cloud classification.

A. Data Description

We evaluated the proposed MKGSL on real multispectral point clouds collected by multispectral LiDAR, named Titan [4]. The dataset contains spectral information at three wavelengths, namely 532, 1064, and 1550 nm. In the original data, the point clouds of the three wavelengths are independent to each other. As described in the previous study, the point cloud of each channel in turn is used as reference data, and the nearest neighbor search algorithm is used to find adjacent points in the point clouds of the other two channels, and the intensity of the other two channels is obtained by the inverse-distance-weighted interpolation method to achieve the fusion of the point clouds [23], [36]. We obtained two multispectral point cloud datasets with three wavelength intensity values $[x, y, z, \lambda_{1550}, \lambda_{1064}, \lambda_{532}]$. The first dataset corresponds to the Harbor of Tobermory (HT), which encompasses a port area measuring 600 m $\times$ 600 m. This dataset was acquired through an online application. The second dataset we utilized is publicly accessible from the 2018 IEEE GRSS Data Fusion Contest and represents the University of Houston (UH) campus, spanning an area of 595 m $\times$ 600 m.

To meet the experimental requirements, we manually segmented the above-mentioned two datasets into 9606 (HT) and 9350 (UH) superpoints based on the point cloud segmentation method [37]. The method specifically combines spatial and spectral similarity metrics to perform point cloud segmentation. By exchanging points between superpoints, it achieves improved segmentation results. To simplify the description, we subsequently refer to the two datasets as HT and UH, respectively. The multispectral point clouds of the two scenes are shown in Fig. 4.

And further labeling was achieved by manually adding labels to the land cover boundaries for the two datasets based on our previous research work [24].

The first dataset is the HT, which covers a port located in Tobermory with dimensions of 600 m $\times$ 600 m. This area contains 7 181 982 points, with an average of 19.9 points per square meter. The second dataset is the UH. We chose data from an area of 595 m $\times$ 600 m to carry out the experiments, and this area consists of 4 436 470 points, with an average of 12.4 points per square meter.

TABLE I
Overall Evaluation Metrics (%) for the Full Scene on the HT Dataset

Method	OA	MP	MR	MF	MIoU
GCN-spatial+spectral [29]	81.36	72.30	61.32	66.36	51.84
GCN-spatial [29]	75.82	68.67	58.55	63.21	46.63
GCN-spectral [29]	76.06	64.30	52.13	57.58	42.03
MLP [35]	79.95	78.08	61.60	68.87	51.92
GAT [31]	84.77	71.71	62.04	66.53	53.08
GCNII [32]	84.83	**79.17**	64.68	71.19	55.96
GCBnet [28]	84.70	77.84	66.58	71.77	57.36
MaSGCN [24]	82.81	69.55	67.71	68.62	54.94
MKGSL(ours)	**88.68**	71.72	**78.03**	**74.74**	**62.08**

The bold values indicate the highest value in the corresponding evaluation metric.

B. Experimental Settings

To evaluate our proposed MKGSL, several representative comparison methods were selected and validated on the two datasets. We calculated the spatial and spectral Euclidean distance matrices for the multispectral point cloud and averaged them after normalization as the adjacency matrix. Afterward, they were input into MLP, GCN, GCNII, GAT, and GCBnet [38] for classification, respectively. To analyze the effect of spatial and spectral information on the classification, two sets of comparisons were setup to validate on GCN using the spectral and spatial Euclidean distance matrices separately as adjacency matrices. Finally, we chose as a comparison with MaSGCN [24], which also uses multiple kernels and is oriented toward multispectral point clouds.

All networks in this article were implemented on the Pytorch platform. The equipment used in the following experiments consists of an Intel (R) Core (TM) CPU i5-12600KF @3.70 GHz and one NVIDIA GeForce RTX 3060 GPU with 12 GB of memory. We calculated the overall-accuracy (OA), macroprecision (MP), macrorecall (MR), macro-F1-score (MF), and MIoU of the classification results to measure the classification performance. And we also calculated precision, recall, F1-score, and IoU for each class.

In our MKGSL method, we utilized ten Gaussian kernels with σ_m values ranging from 0.1 to 1. These kernels were instrumental in capturing various levels of detail. In addition, the hyperparameters in the overall loss function were carefully set. Specifically, α was assigned a value of 5×10^{-4}, β was set to 0.5, γ to 0.1, and λ to 1×10^{-4}. To ensure optimal performance, all methods underwent training for 2000 epochs.

Limited by the memory capacity of the experimental platform, we can only segment the multispectral point cloud into superpoints which must not exceed 10 000. All evaluation metrics were calculated after mapping the classification results back to the original points. To overcome the problem of uneven samples, we counted the number of samples in each class in our experiments, selected 10% of them as training samples, and set different loss weights for each class, i.e., the cube root of the inverse of the proportion of the number of samples in each class to the number of total samples. In the end, we calculated separate

TABLE II
EVALUATION METRICS (%) FOR EACH CLASS ON THE HT DATASET

Method	Metrics	Barren	Building	Car	Grass	Powerline	Road	Ship	Tree	Water
GCN-spatial+spectral [29]	Precision	**75.50**	72.88	33.42	87.70	66.37	82.38	57.34	83.85	91.24
	Recall	82.45	69.97	20.24	81.09	4.89	**70.57**	34.61	99.20	88.85
	F1-score	**78.82**	71.39	25.21	84.27	9.11	76.02	43.16	90.88	90.03
	IoU	**65.04**	55.51	14.42	72.81	4.77	61.31	27.52	83.29	81.86
GCN-spatial [29]	Precision	47.69	72.14	40.04	69.36	52.55	74.70	78.33	86.01	97.17
	Recall	72.12	56.42	**59.07**	53.31	6.63	52.90	36.18	97.56	92.80
	F1-score	57.41	63.32	**47.73**	60.28	11.77	61.94	49.49	91.42	94.93
	IoU	40.26	46.32	**31.35**	43.15	6.25	44.86	32.88	84.20	90.36
GCN-spectral [29]	Precision	66.78	59.39	14.32	**90.95**	73.31	84.09	42.04	80.60	67.23
	Recall	83.61	69.07	6.87	78.29	14.49	56.92	21.13	98.93	39.82
	F1-score	74.26	63.86	9.29	84.15	24.20	67.88	28.12	88.83	50.01
	IoU	59.05	46.91	4.87	72.63	13.76	51.38	16.36	79.90	33.35
MLP [35]	Precision	55.41	**94.14**	39.68	90.87	78.86	**92.94**	77.22	82.17	91.46
	Recall	**88.26**	68.07	36.33	66.45	24.50	55.21	17.86	**99.61**	98.07
	F1-score	68.08	79.01	37.93	76.77	37.39	69.27	29.01	90.05	94.65
	IoU	51.61	65.30	23.40	62.29	22.99	52.99	16.97	81.90	89.85
GAT [31]	Precision	72.37	71.53	29.14	88.46	51.50	79.46	70.75	92.60	89.59
	Recall	79.67	69.64	18.86	82.95	21.48	67.78	35.53	98.98	83.46
	F1-score	75.85	70.57	22.90	85.62	30.32	73.16	47.31	95.68	86.42
	IoU	61.09	54.53	12.93	74.85	17.87	57.67	30.98	91.72	76.08
GCNII [32]	Precision	71.42	79.15	38.97	88.60	**82.17**	88.57	**82.58**	89.35	91.71
	Recall	85.88	77.71	28.40	88.44	9.12	67.80	31.06	99.40	94.29
	F1-score	77.99	78.42	32.86	**88.52**	16.42	**76.80**	45.14	94.11	92.98
	IoU	63.92	64.50	19.66	**79.41**	8.94	**62.34**	29.15	88.87	86.89
GCBnet [38]	Precision	62.48	90.04	**42.23**	88.37	69.87	91.39	75.02	90.54	90.63
	Recall	85.51	69.97	32.96	81.76	41.27	58.92	32.42	99.33	97.02
	F1-score	72.21	78.75	37.02	84.94	**51.89**	71.65	45.27	94.73	93.71
	IoU	56.50	64.95	22.72	73.82	**35.04**	55.83	29.26	89.99	88.17
MaSGCN [24]	Precision	59.29	81.43	40.32	71.74	41.06	73.88	67.51	94.90	95.82
	Recall	71.21	73.56	57.01	67.02	33.76	55.67	56.19	97.41	97.60
	F1-score	64.70	77.29	47.23	69.30	37.05	63.50	**61.33**	96.13	96.70
	IoU	47.82	62.99	30.92	53.02	22.74	46.52	**44.23**	92.56	93.62
MKGSL(ours)	Precision	68.30	82.48	38.24	84.97	45.70	92.74	37.47	**97.77**	**97.79**
	Recall	81.74	**85.78**	58.78	**90.83**	**57.14**	62.46	**68.14**	98.03	**99.35**
	F1-score	74.42	**84.10**	46.34	87.81	50.78	74.65	48.35	**97.90**	**98.57**
	IoU	59.26	**72.56**	30.16	78.26	34.03	59.55	31.88	**95.89**	**97.17**

The bold values indicate the highest value in the corresponding evaluation metric.

TABLE III
OVERALL EVALUATION METRICS(%) FOR THE FULL SCENE ON THE UH DATASET

Method	OA	MP	MR	MF	MIoU
GCN-spatial+spectral [29]	67.39	67.76	54.30	60.29	42.89
GCN-spatial [29]	64.96	70.44	56.70	62.83	43.77
GCN-spectral [29]	60.22	63.82	47.88	54.71	36.07
MLP [35]	59.66	72.48	54.78	62.40	39.93
GAT [31]	61.31	66.31	50.87	57.57	38.81
GCNII [32]	66.80	72.75	58.29	64.72	46.52
GCBnet [38]	69.47	**75.26**	62.37	68.21	50.95
MaSGCN [24]	64.53	68.48	57.86	62.72	45.03
MKGSL(ours)	**79.74**	68.94	**69.13**	**69.04**	**55.78**

The bold values indicate the highest value in the corresponding evaluation metric.

evaluation metrics for each class and made a visual presentation of the classification results.

C. Numerical and Visual Comparison Analysis

The numerical comparison and visual presentation were carried out on the two datasets. The visualization of the experimental results on HT dataset is shown in Fig. 5. The overall evaluation metrics for the full scene are shown in Table I. The proposed MKGSL achieved an OA of 88.68%, an MP of 71.72%, an MR of 78.03%, an MF of 74.74%, and an MIoU of 62.08%.

In order to intuitively analyze the contribution of spatial and spectral information for the classification of multispectral point clouds, we compared GCN-spatial+ spectral, GCN-spatial, and GCN-spectral. Table I shows that the classification performance of the graphs constructed jointly using spatial and spectral information is significantly higher than either one alone. Comparing the visualization using spatial or spectral information alone shown in Fig. 5, it is intuitive to conclude that the graph of spatial information tends to classify points in the close neighborhood into the same class and have difficulty distinguishing fine boundaries, while the graph of spectral information is able to distinguish finer land cover, but the classification results present severe noise interference.

Based on the above-mentioned findings, comparing MLP, GCN, GCNII, GAT, GCBnet, MaSGCN with the proposed MKGSL, MKGSL can significantly improve the classification performance. Specifically, OA improved by 3.84%, MP dropped by 7.45%, MR improved by 10.31%, MF improved by 2.97%, and MIoU improved by 4.72%. And the separate evaluation metrics for each class are shown in Table II. The proposed MKGSL outperforms other methods in most classes but does not perform well in some classes, i.e., car, powerline, and ship. Comparing the visualization results of the above-mentioned methods, MKGSL performs significantly better than the other

TABLE IV
EVALUATION METRICS (%) FOR EACH CLASS ON THE UH DATASET

Method	Class	Barren	Car	Commercial	Grass	Road	Powerline	Residential	Tree
GCN-spatial+spectral [29]	Precision	54.13	36.22	70.84	81.62	76.47	70.78	74.60	77.39
	Recall	80.05	15.41	49.31	74.47	51.76	16.41	51.94	95.05
	F1-score	64.59	21.63	58.14	77.88	61.73	26.64	61.24	85.32
	IoU	47.70	12.12	40.99	63.77	44.65	15.37	44.13	74.39
GCN-spatial [29]	Precision	49.88	64.44	71.15	79.21	74.44	66.60	85.88	71.95
	Recall	82.80	19.50	72.52	66.03	48.36	23.45	47.65	93.33
	F1-score	62.25	29.94	71.83	72.02	58.63	34.69	61.29	81.26
	IoU	45.19	17.60	56.04	56.27	41.47	20.98	44.19	68.43
GCN-spectral [29]	Precision	35.88	28.26	48.86	85.43	77.87	**86.61**	69.12	78.49
	Recall	83.53	10.09	21.06	76.80	45.93	16.81	34.50	94.31
	F1-score	50.20	14.87	29.43	80.88	57.78	28.15	46.03	85.68
	IoU	33.51	8.03	17.25	67.90	40.63	16.38	29.89	74.94
MLP [35]	Precision	34.14	**65.53**	79.58	**90.63**	**87.79**	83.33	82.70	56.12
	Recall	**89.19**	15.79	61.53	70.50	45.22	12.02	48.93	95.07
	F1-score	49.38	25.44	69.40	79.31	59.69	21.01	61.48	70.58
	IoU	32.79	14.58	53.14	65.71	42.54	11.74	44.39	54.54
GAT [31]	Precision	38.88	55.28	59.79	80.38	77.53	62.68	79.12	76.85
	Recall	80.00	12.65	31.70	74.45	47.13	20.40	46.77	93.85
	F1-score	52.33	20.59	41.43	77.30	58.62	30.78	58.79	84.50
	IoU	35.44	11.48	26.13	63.00	41.47	18.19	41.63	73.16
GCNII [32]	Precision	44.95	45.80	**81.14**	84.53	85.18	81.93	77.36	81.10
	Recall	83.79	13.00	59.87	73.33	49.13	22.34	68.81	**96.07**
	F1-score	58.51	20.26	68.90	78.53	62.31	35.10	72.83	87.95
	IoU	41.35	11.27	52.56	64.65	45.26	21.29	57.27	78.50
GCBNet [38]	Precision	46.94	60.35	80.20	87.11	85.25	72.86	83.07	86.28
	Recall	85.38	20.16	71.41	**78.00**	46.53	30.04	71.46	95.97
	F1-score	60.58	**30.22**	75.55	**82.30**	60.20	42.54	76.83	90.87
	IoU	43.45	**17.80**	60.71	**69.93**	43.06	27.02	62.37	83.26
MaSGCN [24]	Precision	43.20	39.28	72.71	85.18	78.14	64.96	**86.02**	78.32
	Recall	80.52	20.97	73.93	66.49	42.97	**33.89**	49.76	94.35
	F1-score	56.23	27.35	73.31	74.68	55.45	**44.54**	63.05	85.59
	Io1U	39.11	15.84	57.87	59.59	38.36	**28.65**	46.04	74.81
MKGSL(ours)	Precision	**75.32**	20.85	75.10	88.16	75.57	40.90	82.94	**92.70**
	Recall	83.17	**41.80**	**83.75**	74.78	**67.55**	29.04	**80.10**	92.84
	F1-score	**79.05**	27.82	**79.19**	80.92	**71.33**	33.96	**81.50**	**92.77**
	IoU	**65.36**	16.16	**65.55**	67.96	**55.44**	20.46	**68.77**	**86.52**

The bold values indicate the highest value in the corresponding evaluation metric.

methods in the classification of land cover boundaries, especially in the discrimination between barren, grass, and road, the contour distinguishing of building. The confusion matrices of the different methods are shown in Fig. 6, from which it can be concluded that MKGSL presents significant difficulties in distinguishing among barren, car, with road and between powerline with tree.

Experiments on UH dataset show similar results, and a visualization of the experimental results is shown in Fig. 7. The overall evaluation metrics are shown in Table III. The proposed MKGSL achieved an OA of 79.74%, an MP of 68.94%, an MR of 69.13%, an MF of 69.04%, and an MIoU of 55.78%. According to Fig. 7, the results of the three groups of GCN-spatial + spectral, GCN-spatial, and GCN-spectral on UH dataset are consistent with those on the HT dataset, and the best performance is achieved by the graph of joint spatial–spectral information. Similarly, the graphs constructed from spatial information present a regionalized classification result, while the graphs constructed from spectral information are more refined but more chaotic.

Comparing with MLP, GCN, GCNII, GAT, GCBnet, MaSGCN, our proposed MKGSL can significantly improve the classification performance. MKGSL outperforms other methods overall. OA improved by 10.28%, MP dropped by 6.31%, MR increased by 6.76%, MF increased by 0.83%, and MIoU increased by 4.83%. Table IV further gives the separate evaluation metrics for each class. MKGSL again performs well in most classes, outperforming other methods except grass and powerline. From the visualization results, as shown in Fig. 7, it can be seen that all methods perform poorly in the car park region in the top right corner of the scene. Apart from this, MKGSL performs significantly better than the other methods in distinguishing the land cover boundaries. The confusion matrices on the UH dataset are shown in Fig. 8. It can be seen that all the methods reflect varying degrees of misclassification between barren and car. This situation is particularly severe on the MKGSL, which contributes to poor precision. However, the visualization in Fig. 7 shows that the MKGSL results are more in line with reality. This indicates a certain contradiction between the evaluation metrics of the classification and the actual classification results.

D. Discussion

By analyzing the visualization and confusion matrix, the misclassifications mainly occur at the boundaries of barren, grass, road, and car, between powerline and tree, and the water region. The possible reason for the misclassification exhibited by MKGSL is that the proposed MKGSL is more sensitive to spectral information. However, the spectral differences among

the boundaries of barren, grass, and road are not significant. Misclassification may be caused by the class boundaries themselves, furthermore the point cloud superpoint segmentation also has an effect. The spatial distribution of some of the powerline overlaps with trees and is spectrally disturbed by trees, and the body of water will absorb some of the lasers which results in a multispectral point cloud with high spectral uncertainty on the water surface. However, for the boundaries of the car, on the one hand, this is due to the fact that the cars themselves have complex spectral information and are partly very close to barren. On the other hand, car is generally small, and experiments on UH dataset even show contradictions between the evaluation metrics and the visualization results.

To analyze the reasons for this issue, the superpoint segmentation needs to be focused on. Before performing the classification, due to the GPU memory limitation of the experimental platform, we segmented the multispectral point cloud into superpoints. The label of a superpoint is derived from a vote of the labels of all the points that have been grouped into the corresponding superpoint. So as long as points of different classes are grouped into the same superpoint, regardless of the label, the upper limit of classification accuracy will definitely be reduced. To address this, we mapped the superpoint labels derived from the voting onto the original point cloud and counted the correctness of the points by comparing them with ground truth, which is an upper limit on the accuracy of the final classification of the subsequent classification methods. And the visualization of the upper limits of classification accuracy for both datasets and the confusion matrices are shown in Fig. 9. It demonstrates that the MKGSL classification results are close to the upper limit of classification due to superpoint segmentation. The distributions of the values in confusion matrices are also highly consistent. Part of the misclassifications of MKGSL can therefore be attributed to insufficient superpoint segmentation, which is particularly evident in the experiments on UH dataset.

V. Conclusion

This article proposes a novel multispectral point cloud classification method named MKGSL. The proposed MKGSL is based on graph theory, which has better characterization capabilities for non-Euclidean data. The proposed MKGSL adaptively maps multispectral point clouds to Hilbert space by using a linear combination of multiple base kernels and designs several prior constraints based on manual experience to guide the evolution of the graph structure, resulting in an intrinsic characterization of the multispectral point cloud for classification. MKGSL makes full use of the spectral information of multispectral point clouds while exploring the intrinsic relationships of point cloud in high-dimensional feature space, providing a new idea to improve the classification performance of multispectral point cloud. Experimental results on two real multispectral point cloud datasets confirm that the adaptively learned graph is able to better characterize the intrinsic properties of land covers and the proposed MKGSL achieves better classification performance compared to other state-of-the-art methods. The incorporation of uncertainty-guided trustworthy fusion into RGBT semantic segmentation has yielded promising results [39]. This research direction holds great significance and contributes to enhancing the classification trustworthiness of multispectral point clouds. Moving forward, we plan to conduct further research in this area.

References

[1] B. Luo et al., "Target classification of similar spatial characteristics in complex urban areas by using multispectral LiDAR," *Remote Sens.*, vol. 14, no. 1, p. 238, 2022.

[2] N. Ekhtari, C. Glennie, and J. C. Fernandez-Diaz, "Classification of airborne multispectral LiDAR point clouds for land cover mapping," *IEEE J. Sel. Topics Appl. Earth Observ. Remote Sens.*, vol. 11, no. 6, pp. 2068–2078, Jun. 2018.

[3] Z. Wu, S. Pan, F. Chen, G. Long, C. Zhang, and S. Y. Philip, "A comprehensive survey on graph neural networks," *IEEE Trans. Neural Netw. Learn. Syst.*, vol. 32, no. 1, pp. 4–24, Jan. 2021.

[4] J. C. Fernandez-Diaz et al., "Capability assessment and performance metrics for the titan multispectral mapping LiDAR," *Remote Sens.*, vol. 8, no. 11, p. 936, 2016.

[5] K. Bakuła, P. Kupidura, and Ł. Jełowicki, "Testing of land cover classification from multispectral airborne laser scanning data." international archives of the photogrammetry," *Remote Sens. Spatial Inf. Sci.*, vol. 41, 2016.

[6] Y. Yang, C. Feng, Y. Shen, and D. Tian, "FoldingNet: Point cloud auto-encoder via deep grid deformation," in *Proc. IEEE Conf. Comput. Vis. Pattern Recognit.*, 2018, pp. 206–215.

[7] Y. Wang and Y. Gu, "Multispectral-LiDAR data fusion via multiple kernel learning for remote sensing classification," in *Proc. 9th Workshop Hyperspectral Image Signal Process. Evol. Remote Sens.*, 2018, pp. 1–6.

[8] Y. Gu, Q. Wang, X. Jia, and J. A. Benediktsson, "A novel MKL model of integrating LiDAR data and MSI for urban area classification," *IEEE Trans. Geosci. Remote Sens.*, vol. 53, no. 10, pp. 5312–5326, Oct. 2015.

[9] F. Ghaseminik, H. Aghamohammadi, and M. Azadbakht, "Land cover mapping of urban environments using multispectral LiDAR data under data imbalance," *Remote Sens. Appl. Soc. Environ.*, vol. 21, 2021, Art. no. 100449.

[10] L. Matikainen, K. Karila, J. Hyyppä, P. Litkey, E. Puttonen, and E. Ahokas, "Object-based analysis of multispectral airborne laser scanner data for land cover classification and map updating," *ISPRS J. Photogrammetry Remote Sens.*, vol. 128, pp. 298–313, 2017.

[11] S. Pan, H. Guan, Y. Yu, J. Li, and D. Peng, "A comparative land-cover classification feature study of learning algorithms: DBM, PCA, and RF using multispectral LiDAR data," *IEEE J. Sel. Topics Appl. Earth Observ. Remote Sens.*, vol. 12, no. 4, pp. 1314–1326, Apr. 2019.

[12] S. Pan et al., "Land-cover classification of multispectral LiDAR data using CNN with optimized hyper-parameters," *ISPRS J. Photogrammetry Remote Sens.*, vol. 166, pp. 241–254, 2020.

[13] Y. Yu et al., "A hybrid capsule network for land cover classification using multispectral LiDAR data," *IEEE Geosci. Remote Sens. Lett.*, vol. 17, no. 7, pp. 1263–1267, Jul. 2020.

[14] Y. Yu et al., "Land cover classification of multispectral LiDAR data with an efficient self-attention capsule network," *IEEE Geosci. Remote Sens. Lett.*, vol. 19, 2022, Art. no. 6501505.

[15] Q. Wang and Y. Gu, "A discriminative tensor representation model for feature extraction and classification of multispectral LiDAR data," *IEEE Trans. Geosci. Remote Sens.*, vol. 58, no. 3, pp. 1568–1586, Mar. 2020.

[16] B. Chen et al., "Multispectral LiDAR point cloud classification: A two-step approach," *Remote Sens.*, vol. 9, no. 4, p. 373, 2017.

[17] J. Sun, S. Shi, B. Chen, L. Du, J. Yang, and W. Gong, "Combined application of 3D spectral features from multispectral LiDAR for classification," in *Proc. IEEE Int. Geosci. Remote Sens. Symp.*, 2017, pp. 5264–5267.

[18] Z. Zhang, T. Li, X. Tang, X. Lei, and Y. Peng, "Introducing improved transformer to land cover classification using multispectral LiDAR point clouds," *Remote Sens.*, vol. 14, no. 15, p. 3808, 2022.

[19] Y. Yu et al., "CAPVIT: Cross-context capsule vision transformers for land cover classification with airborne multispectral LiDAR data," *Int. J. Appl. Earth Observation Geoinformation*, vol. 111, 2022, Art. no. 102837.

[20] Z. Jing et al., "Multispectral LiDAR point cloud classification using se-pointnet," *Remote Sens.*, vol. 13, no. 13, p. 2516, 2021.

[21] C. R. Qi, H. Su, K. Mo, and L. J. Guibas, "PointNet: Deep learning on point sets for 3D classification and segmentation," in *Proc. IEEE Conf. Comput. Vis. Pattern Recognit.*, 2017, pp. 652–660.

[22] C. R. Qi, L. Yi, H. Su, and L. J. Guibas, "PointNet++: Deep hierarchical feature learning on point sets in a metric space," *Adv. Neural Inf. Process. Syst.*, vol. 30, 2017.
[23] P. Zhao et al., "Airborne multispectral LiDAR point cloud classification with a feature reasoning-based graph convolution network," *Int. J. Appl. Earth Observ. Geoinf.*, vol. 105, 2021, Art. no. 102634.
[24] Q. Wang, Y. Gu, M. Yang, and C. Wang, "Multi-attribute smooth graph convolutional network for multispectral points classification," *Sci. China Technol. Sci.*, vol. 64, no. 11, pp. 2509–2522, 2021.
[25] D. Li et al., "Building extraction from airborne multi-spectral LiDAR point clouds based on graph geometric moments convolutional neural networks," *Remote Sens.*, vol. 12, no. 19, p. 3186, 2020.
[26] D. Li et al., "AGFP-Net: Attentive geometric feature pyramid network for land cover classification using airborne multispectral LiDAR data," *Int. J. Appl. Earth Observ. Geoinf.*, vol. 108, 2022, Art. no. 102723.
[27] J. Yang, B. Luo, R. Gan, A. Wang, S. Shi, and L. Du, "Multiscale adjacency matrix CNN: Learning on multispectral LiDAR point cloud via multiscale local graph convolution," *IEEE J. Sel. Topics Appl. Earth Observ. Remote Sens.*, vol. 17, pp. 855–870, 2024.
[28] Q. Wang, Z. Zhang, X. Chen, Z. Wang, J. Song, and T. Shen, "Deep spatial graph convolution network with adaptive spectral aggregated residuals for multispectral point cloud classification," *Remote Sens.*, vol. 15, no. 18, 2023.
[29] T. N. Kipf and M. Welling, "Semi-supervised classification with graph convolutional networks," in *Proc. Int. Conf. Learn. Representations*, Apr. 24-26, 2017, pp. 1–14.
[30] S. Zhang, X. Li, M. Zong, X. Zhu, and R. Wang, "Efficient KNN classification with different numbers of nearest neighbors," *IEEE Trans. Neural Netw. Learn. Syst.*, vol. 29, no. 5, pp. 1774–1785, May 2018.
[31] P. Velickovic et al., "Graph attention networks," *stat*, vol. 1050, no. 20, pp. 10–48 550, 2017.
[32] M. Chen, Z. Wei, Z. Huang, B. Ding, and Y. Li, "Simple and deep graph convolutional networks," in *Proc. Int. Conf. Mach. Learn.*, 2020, pp. 1725–1735.
[33] W. Li, Z. Luo, Z. Xiao, Y. Chen, C. Wang, and J. Li, "A GCN-based method for extracting power lines and pylons from airborne LiDAR data," *IEEE Trans. Geosci. Remote Sens.*, vol. 60, 2022, Art. no. 5700614.
[34] H. Zhang and M. Xu, "Graph neural networks with multiple kernel ensemble attention," *Knowl.-Based Syst.*, vol. 229, 2021, Art. no. 107299.
[35] D. E. Rumelhart, G. E. Hinton, and R. J. Williams, "Learning representations by back-propagating errors," *Nature*, vol. 323, no. 6088, pp. 533–536, 1986.
[36] S. Morsy, A. Shaker, and A. El-Rabbany, "Multispectral LiDAR data for land cover classification of urban areas," *Sensors*, vol. 17, no. 5, p. 958, 2017.
[37] Q. Wang et al., "Multispectral point cloud superpoint segmentation," *Sci. China Technol. Sci.*, no. 67, pp. 1–12, 2024.
[38] T. Zhang, X. Wang, X. Xu, and C. L. P. Chen, "GCB-Net: Graph convolutional broad network and its application in emotion recognition," *IEEE Trans. Affect. Comput.*, vol. 13, no. 1, pp. 379–388, Jan.–Mar. 2022.
[39] Q. Wang, C. Yin, H. Song, T. Shen, and Y. Gu, "UTFNet: Uncertainty-guided trustworthy fusion network for RGB-thermal semantic segmentation," *IEEE Geosci. Remote Sens. Lett.*, vol. 20, 2023, Art. no. 7001205.

Qingwang Wang (Member, IEEE) received the Ph.D. degree in information and communication engineering from the Harbin Institute of Technology, Harbin, China, in 2020.

He is currently a Professor with the Faculty of Information Engineering and Automation, Kunming University of Science and Technology, Kunming, China. His research interests include machine learning applications in remote sensing, specializing in using graph neural networks for analyzing hyperspectral images and LiDAR point clouds.

Zifeng Zhang received the B.Eng. degree in automation from Xidian University Xi'an, China, in 2020. He is currently working toward the M.Eng. degree in navigation guidance and control with the Kunming University of Science and Technology, Kunming China.

His research interests include remote sensing and artificial intelligence applications, and deep learning in Earth and atmospheric research. In particular, the use of graph neural networks to realize remote sensing information extraction in multispectral LiDAR.

Jiangbo Huang (Graduate Student Member, IEEE) received the B.S. degree in information and computing science from the Chongqing University of Posts and Telecommunications, Chongqing, China, in 2022. He is currently working toward the M.S. degree in computer systems organization with the School of Information Engineering and Automation, Kunming University of Science and Technology, Kunming, China.

His research interests include machine learning, graph neural networks, and hypergraph neural networks.

Tao Shen (Member, IEEE) received the Ph.D. degree in electrical engineering from the Illinois Institute of Technology, Chicago, IL, USA, in 2013.

He is currently a Professor with the Faculty of Information Engineering and Automation, Kunming University of Science and Technology, Kunming, China. His research interests include intelligent perception and computation, artificial intelligence, blockchain, and industrial Internet.

Yanfeng Gu (Senior Member, IEEE) received the Ph.D. degree in information and communication engineering from the Harbin Institute of Technology (HIT), Harbin, China, in 2005.

He is currently a Professor with the Department of Information Engineering, HIT. He was a Lecturer with the School of Electronics and Information Engineering, HIT, where he was appointed as an Associate Professor in 2006, and enrolled in the first Outstanding Young Teacher Training Program. From 2011 to 2012, he was a Visiting Scholar with the Department of Electrical Engineering and Computer Science, University of California at Berkeley, Berkeley, CA, USA. He has authored more than 60 peer-reviewed articles and four book chapters, and he holds seven patents. His research interests include image processing in remote sensing, machine learning and pattern analysis, and multiscale geometric analysis.

Dr. Gu is an Associate Editor for IEEE TRANSACTIONS ON GEOSCIENCE AND REMOTE SENSING and *Neurocomputing*. He is also a Peer Reviewer for several international journals, such as IEEE TRANSACTIONS ON GEOSCIENCE AND REMOTE SENSING, IEEE TRANSACTIONS ON IMAGE PROCESSING, and *Remote Sensing of Environment*.